



The Society shall not be responsible for statements or opinions advanced in papers or discussion at meetings of the Society or of its Divisions or Sections, or printed in its publications. Discussion is printed only if the paper is published in an ASME Journal. Authorization to photocopy for internal or personal use is granted to libraries and other users registered with the Copyright Clearance Center (CCC) provided \$3/article is paid to CCC, 222 Rosewood Dr., Danvers, MA 01923. Requests for special permission or bulk reproduction should be addressed to the ASME Technical Publishing Department.

Copyright © 1999 by ASME

All Rights Reserved

Printed in U.S.A.

ON THE DEVELOPMENT AND APPLICATION OF THE FRAP® (FAST-RESPONSE AERODYNAMIC PROBE) SYSTEM FOR TURBOMACHINES – PART 1: THE MEASUREMENT SYSTEM



BREAK

Peter Kupferschmied, Pascal Köppel, Christian Roduner, George Gyarmathy

Turbomachinery Laboratory
Institute of Energy Technology
ETH - Swiss Federal Institute of Technology
8092 Zurich, Switzerland
<http://www.frap.ethz.ch>

ABSTRACT

This contribution gives an overview of the current state, performance and limitations of the fast-response aerodynamic probe measurement system (FRAP® System) developed at the Turbomachinery Lab of the ETH Zurich. In particular, the following topics are addressed:

- **Probe technology:** Miniature probes with tip diameter ranging from 0.84 to 1.80 mm (1-sensor and 3-sensor probes respectively) have been developed. New technologies derived from microelectronics and micromechanics have been used to achieve an adequate packaging of the microsensor chips used. Both the sensor packaging and the sensor calibration (time-independent and time-dependent) are crucial issues for the DC accuracy of any measurement.
- **Aerodynamic probe calibration:** The methods used for the sensor calibration and the aerodynamic probe calibration, the pertinent automated test facilities and the processing of the output data are briefly presented. Since these miniature probes are also capable of measuring the mean flow temperature, aspects related to the recovery factor and the self-heating of the probe tip are treated and some recommendations related to sensor selection are given.
- **Measurement system and data evaluation:** The early measurement chain described in GOSSWEILER, KUPFERSCHMIED and GYARMATHY 1995 has evolved into the FRAP® System. This automatic system incorporates dedicated measurement concepts for a higher accuracy and a more efficient operation in terms of time and failures. An overview of the data evaluation process is given.

The FRAP® System has been tested in real-sized turbomachines under industrial conditions within the temperature limits of 140°C imposed by the sensor technology (axial-flow turbofan compressor, axial-flow turbine, centrifugal compressor). These applications confirmed the potential of the system and encouraged its further development. Now, the system is routinely used in the facilities of the Turbomachinery Lab and in occasional measurement campaigns in other laboratories.

Part 2 of this contribution (RODUNER et al.) will focus on the application of the FRAP® System in a transonic centrifugal compressor of the ETH Turbomachinery Laboratory, while Part 3 (KÖPPEL et al.) treats more sophisticated data analysis methods.

NOMENCLATURE

| | |
|-----------|---|
| C_p | non-dimensional pressure coefficient |
| c | flow velocity |
| c_p | specific heat |
| D | diameter |
| FRAP® | fast-response aerodynamic probe (trademark of ETH Zurich) |
| h | enthalpy |
| I | current |
| K | calibration coefficient |
| L | length |
| M | Mach number |
| m | shaft revolutions during data collection; polynomial exponent |
| N | shaft revolutions per second |
| n | number of sensors; polynomial exponent |
| P | power |
| Pr | Prandtl number |
| p | pressure |
| R | resistance |
| r | recovery correction factor |
| S | sensitivity |
| T | temperature |
| t | time |
| U | voltage |
| W | length |
| α | heat transfer coefficient |
| ϕ | yaw angle |
| γ | pitch angle |
| λ | thermal conductivity |
| ξ_D | dissipation power density |
| ν | kinematic viscosity |

Presented at the International Gas Turbine & Aeroengine Congress & Exhibition
Indianapolis, Indiana — June 7–June 10, 1999

This paper has been accepted for publication in the Transactions of the ASME
Discussion of it will be accepted at ASME Headquarters until September 30, 1999

| | |
|------------------------------|--|
| <i>Sub- and superscripts</i> | |
| D | dissipation |
| e | excitation |
| FR | fast-response |
| I | constant current supply |
| N | shaft synchronized |
| tot | total |
| s | sensor |
| stat | static |
| \sim | ensemble-averaged (over rotor revolutions) |

INTRODUCTION

A better understanding of the unsteady flow phenomena such as secondary-flow or rotor-stator interactions is a key to further improvements in turbomachinery. Besides complex CFD methods, modern measurement techniques with time-resolving capabilities are necessary to determine the instantaneous flow quantities. Such systems have to satisfy numerous requirements like bandwidth (high above the blade-passing frequency of typ. 5 to 12 kHz), high spatial resolution, large Mach number range (from 0.1 up to transonic), high measurement accuracy of the flow quantities, good access to the test section, and low disturbances in the investigated flow section. Furthermore, the resistance to higher temperatures and large pressure ranges is of great advantage.

In this context, fast-response aerodynamic probes are a promising alternative to other time-resolved measurement techniques like hot-wire anemometry (e. g. HINZE 1975) or laser techniques (e. g. STRAZISAR 1993). Besides the flow angles, the Mach number and the velocity (and unlike these complementary techniques) fast-response pressure probes can also measure both time-resolved total and static pressures. All these flow quantities are determined from the pressure levels and fluctuations at different points of the probe tip measured with miniature piezoresistive pressure sensor chips (e. g. KERREBROCK et al. 1974 and 1980, HENKA 1983, EPSTEIN 1985, LARGUIER 1985, COOK 1989). Another advantage of fast-response pressure probes compared to hot-wires is the probe robustness and the insensitivity of the calibration to dirt contamination. The easier access to the test section compared to optical methods is an additional asset for fast-response pressure probes.

In the last decade, a fast-response probe measurement system has been developed for turbomachinery at ETH Zurich (GOSSWEILER, KUPFERSCHMIED and GYARMATHY 1995), with the emphasis on a thorough characterization and optimization of all its components. The system has been successfully used in several applications under industrial conditions, e.g. in an axial-flow jet engine compressor, in a centrifugal compressor (RODUNER, KÖPPEL, KUPFERSCHMIED and GYARMATHY 1998), and in an axial-flow turbine. Thanks to the probe design, the sensor technology and adequate measurement concepts used, the present generation of the system named FRAP® (Fast-Response Aerodynamic Probes) allows to determine both the AC and the DC signal parts with a good accuracy (i. e. velocity uncertainty below 1%).

OVERVIEW OF THE MEASUREMENT SYSTEM

The development of a fast-response aerodynamic probe measurement technique at the ETH Turbomachinery Laboratory in the past ten years comprised on the one hand *generic research on sensors, on miniature probe technology, and probe aerodynamics*. On the other hand, applied research targeted the *development of a complete system for time-resolved flow measurements dedicated to turbomachinery*.

Joined efforts on both research paths have lead to the present generation of fast-response aerodynamic probe system, called FRAP®. To achieve the main goals – i. e. the accurate measurement of both AC and DC parts of the flow quantities – the system was divided into three parts:

- *Hardware components*, consisting of sensors, miniature probes, calibration facilities, probe traversing systems, data acquisition electronics, probe monitoring computer system, and data evaluation and analysis computers.
- *Software components*, consisting of calibration software, probe monitoring and measurement software, and data evaluation and analysis software.
- *Methods and concepts*, which include all procedures necessary to prepare and operate the measurement system in an optimized way, to achieve accurate and reliable measurements. These methods are based on a thorough characterization of the properties of all system elements, the objectives of the measurement campaigns and on the experience gained during measurements in turbomachines.

The benefits of experience have been consistently used to improve the software and the hardware elements listed above. A main objective was to facilitate the use of the system by means of software implementations making it suitable for routine measurements.

PRESSURE AND TEMPERATURE MEASUREMENT WITH MINIATURE SENSOR CHIPS

Miniature pressure sensor chips. The requirements in terms of size, pressure sensitivity and the objective of measuring not only the AC but also the DC part of the pressure signal reduce the choice to piezoresistive and to capacitive pressure sensors. Preference is given to the piezoresistive, because it does not require – in contrast to the capacitive principle – any signal conditioning in the close proximity of the sensor.

However, commercially available packaged pressure sensors are too large to fit into really miniature probes. An alternative is offered by raw sensor chips derived from biomedical applications (Fig. 1). This avoids the size increase due to a double packaging. An overview of pressure sensor chip types used in FRAP® probes is given in Tab. 1.

Sensor chip characteristics. Assuming a constant excitation current I_e in the Wheatstone bridge (Fig. 1, right), the output signal voltage depends strongly on the pressure applied on the diaphragm, and weakly on temperature. On the other hand, the excitation voltage U_e is weakly dependent on the pressure, but strongly on temperature (Fig. 2). This enables the pressure sensor to measure also the diaphragm temperature.

Sensor chip selection criteria. Following basic criteria are used to select the appropriate chip type and chip individuals for an application in aerodynamic probes:

- *Sensor geometry and size* in accordance with the general shape and size of the probe tip (see "Optimization of the probe geometry").
- Due to its small size, the sensor diaphragm shows a mechanical eigenfrequency between 500 and 900 kHz. The limiting frequency for turbomachinery measurements (blade-passing frequencies typ. 5 to 12 kHz) may be given by the pneumatic cavity if the sensor is mounted in the probe interior (see "Dynamic sensor calibration").
- *Pressure sensitivity*; normalized with a given excitation current:

$$S_I = \frac{U(\Delta p, T_{Ref}) - U(0, T_{Ref})}{\Delta p \cdot I_e} \left[\frac{mV}{bar \cdot mA} \right] \quad (1)$$

This definition addresses a possible overheating of the sensor diaphragm, which would strongly reduce the pressure signal stability (DC) and increase the error on the measured flow temperature.

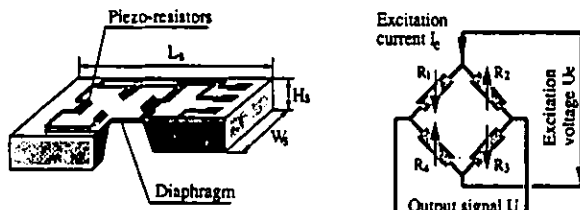


Fig. 1: Piezoresistive miniature pressure sensor chip.

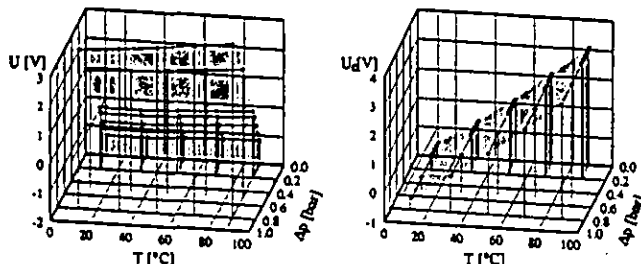


Fig. 2: Typical excitation and output signals of a piezoresistive pressure sensor chip (Sensym P788, $I_e = 1 \text{ mA}$).

| | Keller 1026 | Sensym P788 | NovaSensor NPD240 |
|---|---------------|----------------|-------------------|
| Size (L_s, W_s, H_s) [mm] | 2.0, 1.0, 0.5 | 1.7, 0.6, 0.15 | 1.0, 0.7, 0.2 |
| Surface $L_s \times W_s$ [mm ²] | 2.00 | 1.02 | 0.70 |
| Resistors on diaphragm | 4 | 4 | 2 |
| Bridge resistance R_e | 4.7 kΩ | 5.2 kΩ | 0.8 kΩ |
| Pressure sensitivity S_I ($I_e = 1 \text{ mA}$) [mV/mA bar] | typ. 55 | typ. 70 | typ. 10 |
| Pressure sensitiv. S_{SmW} ($P_D = 5 \text{ mW}$) [mV/bar] | typ. 58 | typ. 67 | typ. 62 |
| Spec. pressure range (linearity range) [mbar] | n.a. | 400 | -65 ... + 400 |
| Excitation voltage U_{eSmW} ($P_D = 5 \text{ mW}$) [V] | ~ 4.8 V | ~ 5.1 V | ~ 2.0 V |
| Dissip. power density ξ_{DSmW} [mW/mm ²] | 2.5 | 4.9 | 7.1 |

Tab. 1: Typ. data of minialure differential pressure sensor chips used in FRAP® probes (monocrystalline silicone at $T \approx 30^\circ\text{C}$).

- Total bridge resistance R_e (cf. Fig. 1, right):

$$R_e = \frac{U_e}{I_e} = \frac{(R_1 + R_4) \cdot (R_2 + R_3)}{R_1 + R_2 + R_3 + R_4} \quad (2)$$

For high-performance applications, it should be noted that higher bridge resistance R_e and long electric connections to the amplifiers affect the amplitude and phase response of the system (Fig. 3).

- Temperature sensitivity: The temperature dependency can be described by the temperature coefficient of the resistance TCR_e

$$TCR_e(T_m) = \frac{1}{R_e(T_m)} \frac{R_e(T_2) - R_e(T_1)}{T_2 - T_1} \quad (3)$$

with $T_m = (T_1 + T_2)/2$. A higher coefficient provides a higher resolution of the diaphragm temperature measurement.

- Stability of the signals: The accurate measurement of both the AC and DC part of the pressure signal relies on stable sensor signals. Remaining errors can be corrected to some extent by applying appropriate concepts during the measurement.
- Dissipation power density: This parameter describes roughly the transfer of the sensor's dissipated heat to the hosting probe tip

$$\xi_{diss} = \frac{P_{diss}}{L_s \cdot W_s} \quad (4)$$

ξ_{diss} should be kept low to avoid an overheating of the sensor diaphragm, which would decrease the sensor stability and the accuracy of the temperature measurement.

- Pressure limitation: Although some preferred sensor chips are designed for differential pressures up to 350 mbar only, they can be used up to several bar. All non-linearities occurring in this case are taken into account in the sensor calibration process. In the following, a full-scale (FS) value of 1 bar is assumed for operating the sensor types presented in Tab. 1.
- Temperature limitation: Most pressure sensor chips mounted in FRAP® probes are machined from monocrystalline silicon. Due to the resistor noise (*p-n-junction*), this material sets an upper limit to the operating temperature at 120°C to 140°C , depending on the doping level. However, the materials used to build the probe (metals, ceramics, adhesives) withstand more than 200°C .

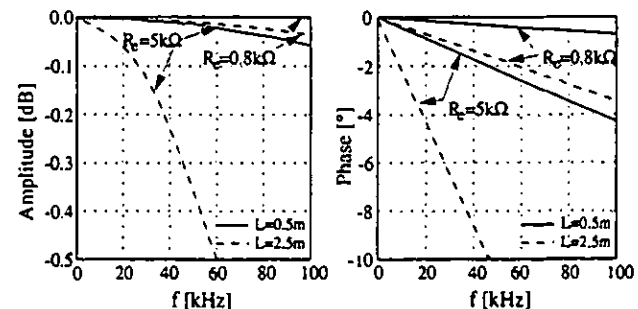


Fig. 3: Alteration of the amplitude and phase response due to the bridge resistance R_e and cable length L (KUPFERSCHMIED 1998).

Development trends. Higher temperature applications require other micromachining techniques for the sensor manufacturing. For example, the commercial availability of a chip based on silicon-on-insulator (SOI) technology with comparable size and properties would allow operating temperatures up to 240°C (e.g. LISEC et al. 1996).

PROBE TECHNOLOGY

Design process

Miniature fast-response probes are designed in an iterative process, which takes aspects from various fields into account. A general flow chart of this process and its interdependencies is shown in Fig. 4. In order to obtain optimal probe characteristics, various development objectives and design criteria have to be carefully balanced:

Mechanical optimization of the probe with respect to the measurement task: Straight shaft geometries are preferentially used in turbo-

machinery in order to facilitate the access to the flow region. Mechanical design is also an issue to estimate the deflection and to prevent the probe from breaking. The following cases are considered: Aerodynamic load, flutter, excitation due to Kármán vortex street, and mechanical excitation induced by the turbomachine (e.g. components, blade passing). A structural analysis has been performed with a finite element program (NASTRAN) for each type of FRAP® probe in order to determine the eigenfrequencies, the modes and the expected bending. This analysis and the experience gained from applications did not reveal any significant vibrations or perturbations of the pressure measurement.

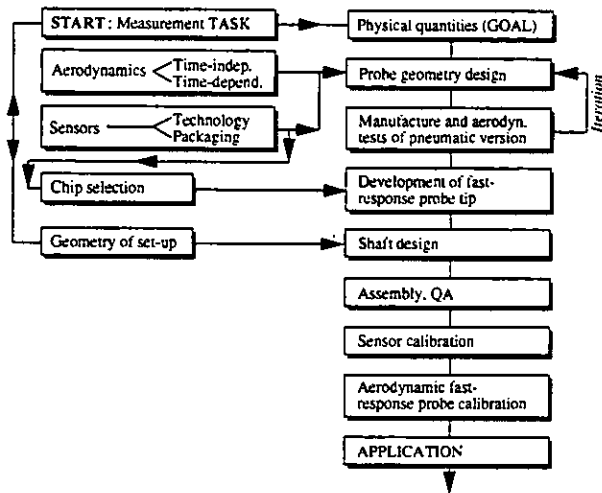


Fig. 4: Fast-response probe design and development steps.

Optimization of the probe geometry: Over the last years, different probe geometries such as cylinders (e.g. KERREBROCK et al. 1974) wedges (e.g. HENEKA 1983), or pyramids (AINSWORTH et al. 1995) have been used for fast-response measurements. The choice of the geometry should not only be dictated by static design considerations derived from pneumatic probes (e.g. CHUE 1975) but also by the time-dependent characteristics (KOVASZNAY et al. 1981). Investigations by HUMM et al. (1995, and HUMM 1996) have demonstrated the strong influence of both geometry and size on the accuracy of the measured time-dependent flow quantities in highly fluctuating flow fields. Therefore, a *cylindrical geometry* was chosen, this being the best compromise for the FRAP® probes for fast-response measurements in fluctuating flows.

- The lower *angular sensitivity* of cylinder as compared to wedge probes does not affect this decision, assuming that a good overall resolution of the pressure measurement is provided. For example, measurements at only $M = 0.2$ with a cylindrical probe (FRAP® C1S18) under industrial conditions showed an angular uncertainty due to the noise over the whole measurement system below 0.04° .
- However, the *angular range of the probe* – i. e. the range in which measurements can still be correctly evaluated – is of great importance. The typically highly fluctuating flows encountered behind rotating turbomachine stages require large yaw angle tolerance ranges for radially traversed probes: Even if yaw angle fluctuations $\Delta\phi_{max}$ of $\pm 20^\circ$ seem to be a typical upper limit for ensemble-average of fluctuations, the required angular range $\Delta\phi_{max}$ may be far larger if multi-sensor probe data are processed as real time series (see “Concepts of Application” and KUPFERSCHMIED 1998).

- In the typical operating range ($Re = 10^3 \dots 10^5$), the *Reynolds dependency* of cylindrical probes remains low for small probe diameters. Corrections might be necessary if the probes are operated under low pressure conditions such as encountered in blow-down facilities.
- The maximum *Mach number* considered for past and present applications of the FRAP® probes was 0.8. The Mach number effect is taken into account with aerodynamic calibrations.

Miniaturization of the probe size: Due to the intrusion of the probes into the flow, a small size generally helps to reduce time-dependent and time-independent interactions with the flow. Experiments by HUMM (1996) have clearly demonstrated that the severe measurement errors due to time dependent effects are directly proportional to probe size. Thus, the size reduction becomes of crucial importance. Furthermore, the *spatial resolution* of the probe increases when the distance between the pressure taps is smaller.

Optimization of sensor properties: This objective is a compromise between the basic sensor properties, the *sensor packaging technique*, and the concepts applied during the measurements. All these elements, and in particular the impact of the minimum probe size on the sensor properties, have been thoroughly investigated. As a consequence, the prototype probes – such as the 4-sensor probe Z4LS25 with an outer diameter of 2.50 mm (e.g. GOSSWEILER et al. 1995) – have evolved toward a second probe generation, designated as FRAP® probes.

Development of FRAP probes

New concepts allowing the manufacturing of small series of probes were necessary for the further miniaturization of these multi-sensor probes. Thus, two types of cylindrical probes with an outer diameter of 1.80 mm have been developed, accommodating 1 and 3 sensors, respectively (Fig. 6, left). A fourth sensor can be implemented into the latter probe type in the future, enabling 3D flow measurements.

The sensor chips are located inside the probe, with the chip diaphragm turned towards the interior (Fig. 5). This avoids damages due to particle impacts on the chip's active side. Thus FRAP® probes were successfully operated over several hundred hours without damages.

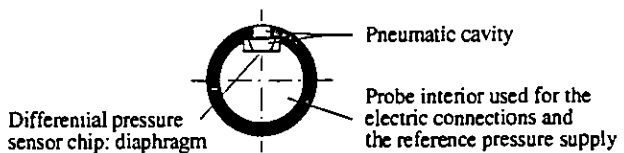


Fig. 5: Schematic view of the sensor chip location in a cylindrical fast-response probe.

Alternative methods for the manufacturing and the *sensor packaging* derived from micromechanics and microelectronics were required to scale the diameter of 3-sensor probes down to 1.8 mm. For example, the geometry of the complex miniature probe parts has to be manufactured within 0.01 mm. Reliable electrical connections of the sensor chips are also important issues considering the complexity of the probe interior.

As shown later (“Measurement concepts”), the probes are operated in the *differential pressure mode*. By supplying the probe interior with a reference pressure close to the common pressure level of the turbomachine, sensors with *per se* small pressure ranges can be utilized (typ. 350 mbar). This mode not only enhances the pressure sensitivity of the sen-

sors, but also allows to readjust the sensor's gain and zero during the application. This is of great advantage for accurate measurement of the DC signal part, considering the limited stability of microsensors due to hysteresis drift effects.

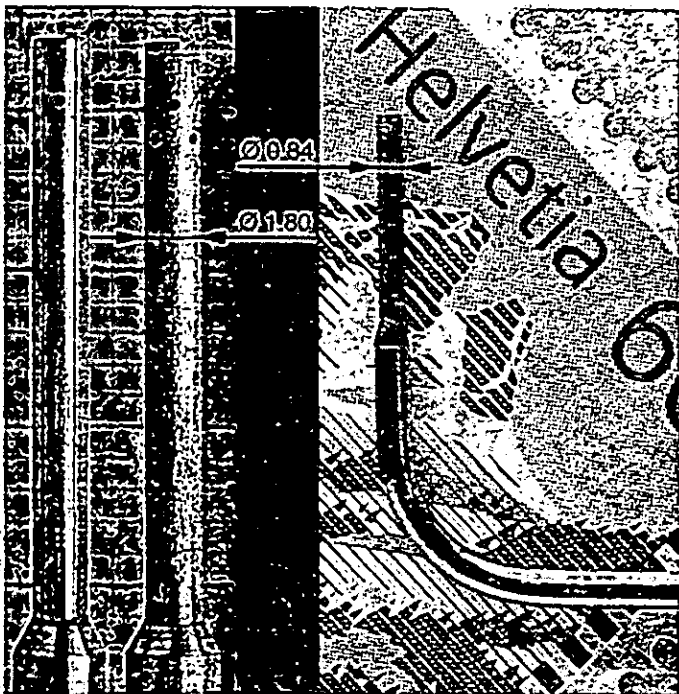


Fig. 6: Left: Tip of a 1 and a 3-sensor probe C1LS18 and C3LS18 (tip: Ø1.80 mm; prismatic shaft: Ø3.0 mm); Right: Tip of 1-sensor Pitot probe P1S08 (diameter 0.84 mm).

For this reason, all FRAP® probe types are equipped with a controlled pressure supply. The smallest fast-response probe using this philosophy is the Pitot with a tip diameter of 0.84 mm (Fig. 6, right). With this design and the type of microsensor used, a sensitivity of typ. 90 mV/bar (at 5 mW excitation power) before amplification can be achieved.

SENSOR CALIBRATION

Introduction. Depending on the time interval considered, different issues are of interest:

- **Static properties:** What is the achievable DC (steady state) accuracy for pressure and temperature? What are the best time intervals before the sensors have to be recalibrated (*long-term properties*)?
- **Dynamic properties:** What is the typical dynamic response of the pressure and the temperature reading?

After the probe manufacturing, the sensors require an accurate calibration in function of temperature, pressure and time. While the calibration under static conditions takes place prior and after each measurement campaign for each probe, the calibration under dynamic conditions – i.e. with higher temperature or pressure gradients – are performed for each type of probes only and used as typical data.

Static sensor calibration

Sensor test facility. A computer-controlled facility has been developed in which completed probes are calibrated automatically in terms of temperature and pressure. The probe tips are held into an environmental

chamber where steady temperature levels are maintained over several hours (level accuracy ± 0.1 K, steadiness within ± 0.02 K). The temperature is cycled according to the temperature range required by the target application. Several successive temperature cycles are necessary to separate drift effects from thermal hysteresis. The reference pressure of the probe inner part is supplied with precision valves in 7 steps from 0 to the required maximum pressure (supply fluctuations: 2.5 Pa/min for a range of 1 bar). The reference pressure is measured with ParoScientific "Digi-quartz" transducers. All electric signals are measured with a digital scanner voltmeter built at the Laboratory (max. absolute error: 50 ppm FS). A steady, low velocity air flow is blown on the probe tips (or sensor chips, respectively) to minimize heat convection effects in the chamber.

Typical results for the pressure signal. The pressure signal zero changes of a sensor in a 3-sensor probe are shown during 3 temperature cycles between 12 and 92 °C and total duration of 510 h in Fig. 7 (Left). The lines between the steps are drawn to make the reading easier. At every temperature step, a pressure cycle with 7 levels was also applied.

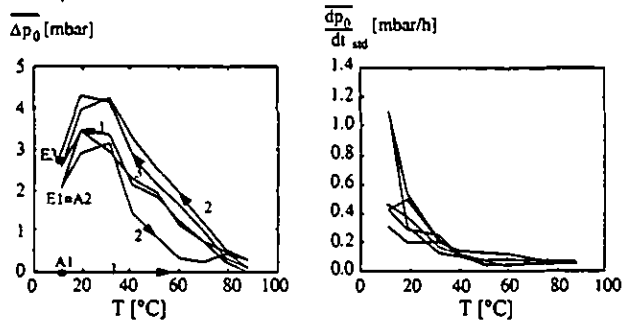


Fig. 7: Pressure signal zero and short-time stability of a typical sensor during 3 temperature cycles (3-sensor probe FRAP® C3S18, $T = 12 \dots 92$ °C, $\Delta t = 510$ h).

All cycle data are represented as differences to the ascending part of the first temperature cycle and can be interpreted as following:

- The plots reveal that the sensor's behavior is subject to a "training" effect: the larger differences between the first and the following loops occur not only when the probe is calibrated for the first time, but also after longer stocking periods at ambient temperature. This effect was also observed in medical catheter manufacturing (MUNTWYLER 1996), but could not be completely explained yet.
- A small thermal hysteresis occurs between the ascending and the descending cycle part. Apart from the first loop, the hysteresis remains within 2 mbar limits over this temperature range.
- A small drift of the zero can be observed from the end points of the loops and amounts to approx. 0.5 mbar in the 2nd and 3rd cycle.
- The short-term stability is defined herein as the pressure-zero change over a short observation period (in [min] or [h]):

$$\frac{dp_0}{dt} (\Delta p=0, T=t) = \frac{p(t_2) - p(t_1)}{t_2 - t_1} \quad (5)$$

The standard deviation of these gradients at each temperature step during all cycles remains generally below 0.5 mbar/h (Fig. 7, right). The increase of stability of the pressure zeroes above 40 °C is of practical interest for turbomachinery applications.

The creep of the pressure reading – i.e. when the probe is submitted to higher pressure levels – amounts to 0.08% FS (1 bar), which is an im-

provement compared to other designs (e.g. COOK 1989: 0.3% FS). No particular procedures are required in the later application, since the fluctuating pressure part (AC) due to the flow remains smaller. The gain of the pressure signal was found to be stable, with changes of only a few per mil per year. Despite the fairly good characteristics of the sensors, the offsets and gains – including the amplifiers and the data acquisition equipment – are routinely readjusted in short time intervals during the measurement process to improve the DC accuracy of the system.

Typical results for the temperature signal. The experience in several turbomachinery applications revealed the interest for an accurate flow temperature information, besides the time-resolved pressure data. While the offset of each pressure signal can be checked and readjusted during measurements by changing the reference pressure in the probe interior, a temperature offset can not easily be detected while the probe is inserted in the machine. Therefore, the stability of the temperature signal had to be carefully investigated. The example in Fig. 8 (left) shows the mean indicated temperature of a 1-sensor probe for 7 temperature cycles, plotted for each step as a difference to the indicated temperature in the ascending part of the first loop.

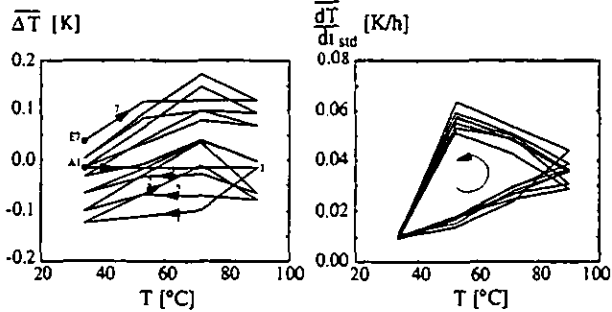


Fig. 8: Long-term stability of the indicated temperature (probe FRAP® C1S18#12, 4 temperature steps of 6 h, $T = 35 \dots 92^\circ\text{C}$).

Compared to the raw sensor chip (i.e. before encapsulation), time-dependent effects can now be noted. However, the mean deviations remain within $\pm 0.15\text{ K}$ during the observation period of 240 h. These results are typical for this type of sensors and probes and small in comparison to other errors arising in the flow temperature measurement.

Sensor self-heating. Due to the power dissipated in the sensor's resistors, the sensor diaphragms are prone to heat up. Since the heat transfer to the surrounding flow depends on the flow velocity, the measured absolute temperature level as well as the pressure signal stability are affected. EPSTEIN (1985) reported about a sensor temperature of 40 to 50°C when the probe was in still air at ambient temperature. To reduce such drawbacks, his probes were then equipped with a cooling system.

In the present case, a cooling would not only be problematic for the probe design (size), but also prevent the measurement of temperature. Therefore, the governing parameters for self-heating have been investigated. For cylindrical probe tip geometries, the self-heating ΔT can be described as (KUPFERSCHMIED et al. 1998):

$$\Delta T = \frac{n R_e I_e^2}{\lambda \pi L} \frac{1}{0.3 + \frac{0.62(c \cdot D/V)^{1/2} Pr^{1/3}}{[I + (0.4/Pr)^{2/3}]^{1/4}}} , \quad (6)$$

with n being the number of sensors and D the tip diameter.

Experiments with several probes are in good agreement with Eq. 6. Cases of constant L (tip length involved in the heat exchange) are shown as lines in Fig. 9. The overtemperature of the 1-sensor probe type in air at only 2 m/s amounts to 0.5 K.

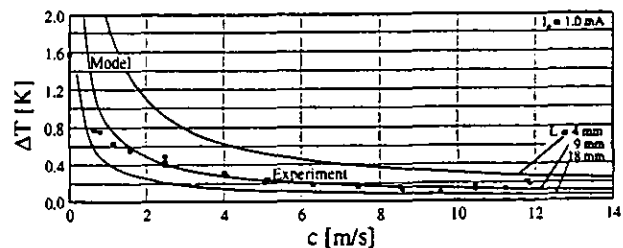


Fig. 9: Overtentperature due to self-heating of a 1-sensor probe (FRAP® C1S18#13) and model results (solid lines).

Dynamic sensor calibration

Pressure calibration. The recessed position of the sensor diaphragm behind the pressure tap (see Fig. 5) defines a pneumatic cavity which affects the dynamic behavior of the pressure signal. For this reason, several configurations of sensor chips and geometries relevant for this kind of probes have been investigated over a high bandwidth using a shock tube. All cylindrical types of FRAP® probes presented herein show amplitude and phase plots with a shape similar to Fig. 10.

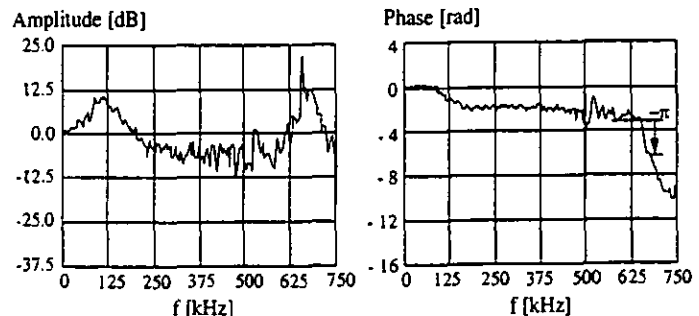


Fig. 10: Dynamic response of a miniature pressure sensor in a recessed cavity (GOSSWEILER, HUMM and KUPFERSCHMIED 1990b).

The first peak reveals the eigenfrequency of the cavity (90...105 kHz, according to the probe type), and the second sharper peak the sensor diaphragm eigenfrequency (650...850 kHz, depend. on sensor type).

An individual calibration of each probe in a frequency range up to 100 kHz can be envisaged for higher requirements in terms of analogue bandwidth, and amplitude and phase accuracy. A numerical correction of the amplitudes and phases can then be applied to the time series in the data evaluation after measurements.

Temperature calibration. The behavior of the pressure and temperature signals under small and large temperature gradients – e.g. occurring during the run-up of a machine or the sudden immersion in hot flows as encountered under surge conditions – has been tested for each probe type. The typical response of the indicated pressure zero is shown in Fig. 11 (left) during a gentle temperature change (max. 4 K/min), and in Fig. 11 (right) for a temperature step of 60 K. A closer view to the data shows that a zero offset of 5 mbar is reached after 10 s. The pressure gain was found to be unaffected by dynamic temperature effects.

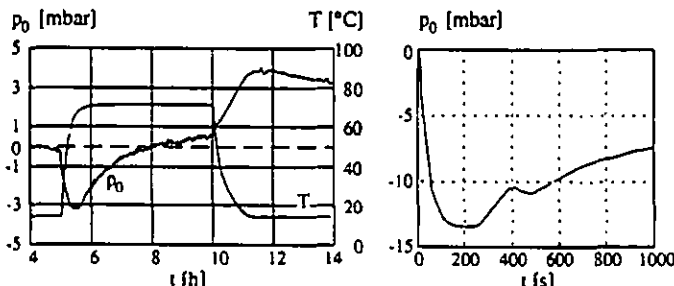


Fig. 11: Indicated pressure zero after temperature changes of ± 60 K and after a step of $+60$ K (probe FRAP® C1S18#12).

The response of the indicated temperature has a first order system behavior (not shown here), with a time constant $\tau_{63\%}$ of 13.8 s for the 1-sensor probe FRAP® C1S18 in low air velocity ($c = 1.5$ m/s). The shorter time constant of 7.5 s of the 3-sensor probe type FRAP® C3S18 is due to the completely different design of the tip interior. The time constants decrease roughly by an order of magnitude if the flow velocity is increased to $M = 0.5$ (other conditions unchanged). The pressure zero offset is also more influenced by temperature steps (Fig. 11, right) and might require a correction when applied in blow-down facilities or under surge conditions with larger temperature variations.

Conclusions. The dynamic pressure response has been quantified for different configurations and a bandwidth of over 500 kHz. In the present applications with an analogue bandwidth of 44 kHz, the signals do not require any corrections. However, the pressure signals could be corrected with the sensor transfer functions for higher requirements regarding the analogue bandwidth or the amplitude and phase accuracy.

The effects of temperature transients on the indicated pressure zero are rather small. A further strong reduction can be achieved by applying adequate operating concepts during the measurements (see below). Depending on the magnitude of the temperature fluctuations occurring during surge, a correction of the measured pressure zero based on experimental data may become necessary. Due to structural integrity of the probe components the flow temperature should not exceed 200 °C over time periods longer than 0.5 seconds.

Finally, the time-constant of the indicated temperature (approx. 1 s at $M = 0.5$) confines the probes to mean flow temperature measurements. Other techniques such as aspirating or cold wire probes are necessary for time-resolved temperature measurements in turbomachinery (e.g. EPSTEIN and NG 1983, VAN ZANTE et al. 1995, ARTS et al. 1996).

Modeling of the static sensor calibration data

Model-based reconstruction. In contrast to most other pressure sensing applications, no external electronic circuitry is used here to compensate temperature effects on the zero offset and the sensitivity of the pressure signal (MALLON and BERNSTEIN 1983). An active compensation method using a model-based reconstruction is applied (GOSSWEILER et al. 1990a), to enhance the accuracy and to avoid the larger size due to additional circuits. The sensor characteristics $U_e(T, \Delta p)$ and $U(T, \Delta p)$ are calibrated over the whole pressure and temperature range of the target application. Their integration into a numerical model enhances the accuracy remarkably.

Therefore, the sensor data $U, U_e = F(\Delta p, T)$ collected during the static calibration are used. In particular, the cycle with the lowest drift

and hysteresis (see general shape in Fig. 7) will be selected. According to the voltage characteristics of piezoresistive pressure sensors (Fig. 2) and after exchanging the dependent and the independent variables, the properties of each sensor can be approximated by a polynomial model:

$$\Delta p(U, U_e) = \sum_{i=0}^m \sum_{j=0}^n k_{pij} U^i U_e^j \quad (7)$$

$$T(U, U_e) = \sum_{i=0}^m \sum_{j=0}^n k_{Tij} U^i U_e^j \quad (8)$$

Model accuracy. In most cases, the use of polynomials of second degree ($m = n = 2$) satisfies the accuracy requirements.

The typical standard deviation of the residuals shown for a 1-sensor probe (Fig. 12) amounts to 0.2 mbar (FS = 1 bar), and 0.04 K (temperature span: 60 K). Using $m = n \geq 2$, the extreme residuals stay below 1 mbar and 0.2 K respectively, see Fig. 12 (right). They contain stochastic as well as systematic measurement errors (partly due to hysteresis and drift) occurring during the calibration. Thus, polynomials of the third degree or above would improve the reconstruction accuracy in special cases only and will not be further considered.

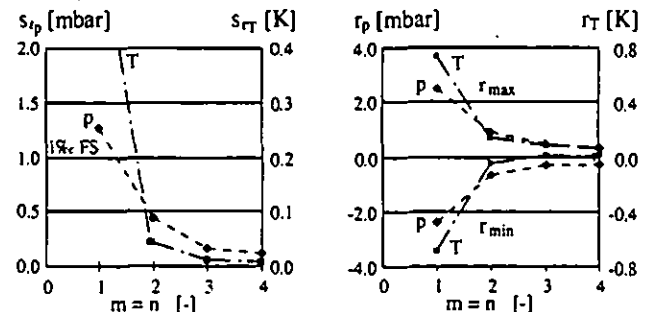


Fig. 12: Reconstructed pressure and temperature signals of probe FRAP® C1S18#12: Standard deviations of the residuals (left), and minimum and maximum residuals (right).

AERODYNAMIC CALIBRATION OF THE PROBES

Introduction. Although a calibration in controlled dynamic flows would be very valuable, no known facilities can provide such conditions in air for frequencies relevant to turbomachinery. Therefore the time-dependent part of the probe aerodynamics has been investigated with large-scale model experiments in water by HUMM et al. (1995), and these considerations are taken into account for the real applications. Correction procedures for dynamic effects on the probes are currently investigated (GIZZI and GYARMATHY 1998).

The calibration discussed here is confined to flows under steady state conditions. The objective to measure also the DC level with good accuracy (i.e. velocity uncertainty $< 1\%$) requires an extensive individual calibration of each fast-response probe in a well-known steady reference flow. Operating conditions such as Mach number must be varied. The angular range is chosen according to the intended application.

Automatic calibration facility. The probes are calibrated in a broad Mach number range up to 0.8 in a free jet nozzle (Fig. 13, left). The components of this facility have been designed to achieve data of an accuracy one order of magnitude higher than required in the target application. Since fast-response probes must cover large angular ranges

with a fine resolution (see "Design process"), meshes with several hundred points are necessary for each probe at any Mach number level.

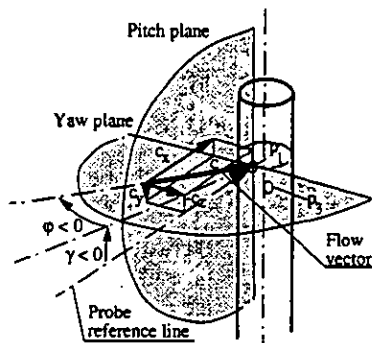
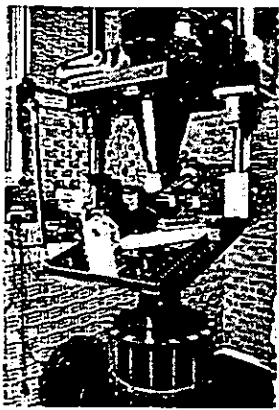


Fig. 13: Vertical-nozzle free jet facility (\varnothing 100 mm) for the calibration of aerodynamic probes. Probe frame of reference: yaw-pitch system (as defined by TREASTER and YOCUM 1979).

To make such time-consuming calibrations feasible, the calibration system is fully computer-controlled. The configuration includes 3-axis probe actuators (angular uncertainty: $\pm 0.03^\circ$), multi-channel pressure monitoring system, voltage scanner for probe sensors signals (abs. uncertainty: ± 50 ppm FS) and thermistors (abs. uncertainty: 0.1 K). A separate control unit is dedicated to the centrifugal compressor air supply. The air flow temperature is controlled within ± 0.05 K (at $0.2 < M < 0.7$) to avoid transient temperature effects on the probe's miniature sensors.

A calibration rate of 800 angular positions per hour can be achieved with fast-response probes. The rate with pneumatic probes is lower (120 pos./h), since pressure-lead transients have to decrease before the measurements are taken (these time delays are controlled by a statistical algorithm based on the standard deviations of the pressure samples). For example, the calibrated pressure coefficients C_p of a conventional pneumatic probe such as the 3-hole probe C3P18 having the same external geometry as the 3-sensor probe FRAP® C3S18 are shown in Fig. 14. The overall repeatability of the C_p is typically better than $\pm 2\%$.

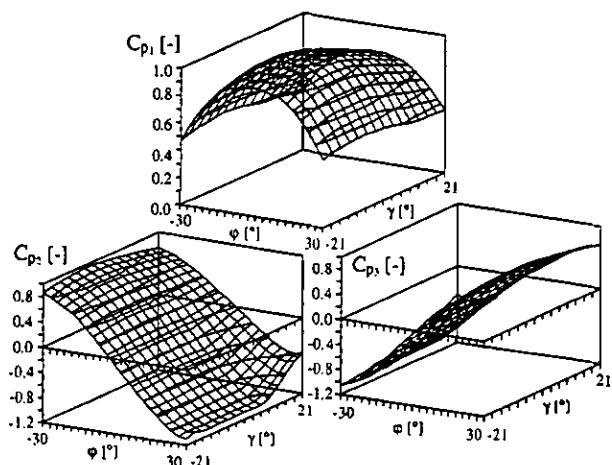


Fig. 14: Aerodynamic coefficients of a 3-hole probe (C3S18P, $\varnothing 1.80$ mm, $M = 0.30$). Each mesh node is a calibration point. The frame of reference of the probe is defined in Fig. 13 (right).

Calibration of the recovery factor

To prepare the probes for measuring the (time-averaged) flow temperature additionally to the time-resolved pressure, the recovery factor r

$$r = \frac{h_i - h_{stat}}{h_{tot} - h_{stat}} = F(M, T_{stat}) \quad (9)$$

has to be calibrated in the jet nozzle in terms of Mach number and static temperature. The range of temperature is limited by the nozzle facility to $15^\circ\text{C} \leq T_{stat} \leq 70^\circ\text{C}$. The difference between the total flow temperature and the temperature indicated by a 1-sensor probe is plotted in Fig. 15 for two typical yaw positions of the probe (stagnation point and angle where the static pressure is approximately measured). The corresponding recovery factor can be obtained by using the nozzle velocity c_F and the specific heat c_p as:

$$r = 1 - \frac{2c}{c_F^2} \cdot (T_{tot} - T_i) . \quad (10)$$

Whereas the dashed line $T_{tot} - T_{stat}$ in Fig. 15 illustrates an (ideal) stagnation-point recovery factor of 1, the recovery factor of the 1-sensor probe type FRAP® CIS18 (grey lines in Fig. 15) corresponds to a recovery factor of about 0.6. This much lower value is due to heat conduction in the probe interior. Based on its definition (Eq. 10), the uncertainty of the recovery factor increases strongly for low velocities where the temperature head $T_{tot} - T_{stat}$ is low. Therefore the range below $M = 0.2$ should be disregarded (SMOOTH 1996 even recommends $M = 0.3$ as a lower limit).

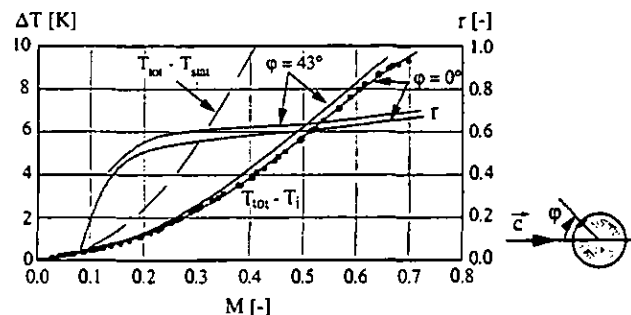


Fig. 15: Difference between flow total temperature and indicated probe temperature; resulting recovery factor (FRAP® C1S18#12).

Modeling of the static aerodynamic probe calibration data

Aerodynamic coefficients. The calibration coefficients C_p obtained for every probe pressure tap are combined into an appropriate set of non-dimensional aerodynamic coefficients to allow the evaluation of the physical flow quantities in the application. The choice of these coefficients is depending upon the probe geometry. For the present cylindrical probes, the coefficients have been chosen according to KRAUSE and DUDZINSKI (1969). The yaw sensitivity is described by:

$$K_\phi = \frac{P_2 - P_3}{P_1 - P_m} = K_\phi(\phi, \gamma, M) , \text{ with } p_m = \frac{P_2 + P_3}{2} \quad (11)$$

The pitch sensitivity can be obtained by adding a fourth sensor in the 3-sensor probe shown above (or by using the 4-sensor probe Z4LS2.5 presented in GOSSWEILER, KUPFERSCHMIED and GYARMATHY 1995), enabling it to make 3D measurements:

$$K_\gamma = \frac{P_2 - P_3}{P_1 - P_m} = K_\gamma(\phi, \gamma, M) . \quad (12)$$

The total pressure and static dependencies are given by

$$K_{tot} = \frac{P_{tot} - P_1}{P_1 - P_m} = K_{tot}(\phi, \gamma, M) \text{ and} \quad (13)$$

$$K_{stat} = \frac{P_{stat} - P_1}{P_1 - P_m} = K_{stat}(\phi, \gamma, M) . \quad (14)$$

Since all coefficients also depend upon the Mach number, the calibration is performed for several Mach number steps. In the Reynolds number range considered ($Re_S \approx 10^3 \dots 1.2 \cdot 10^5$), viscosity effects have only a marginal influence for this probe geometry, making a variation of Re unnecessary.

The angular range in which data can be evaluated is limited by the denominator $p_1 \cdot p_m$, which shows numerical poles at yaw angles ϕ of approx. $\pm 40^\circ$ for the cylindrical geometry with the given tap locations (Fig. 16). Basically, a data evaluation beyond the poles is possible. However, the solutions become ambiguous and must be identified and treated accordingly (KUPFERSCHMIED 1998).

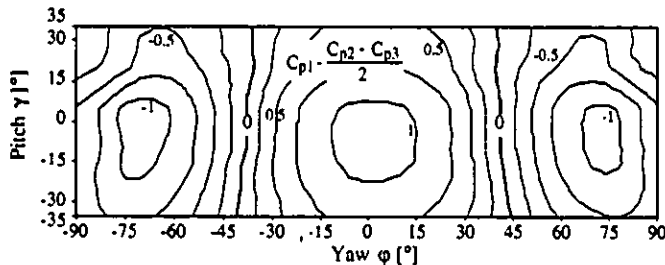


Fig. 16: Angular distribution with poles (zero lines) of the denominator $C_{p1} - (C_{p2} + C_{p3})/2$ of a 3-hole probe C3P18.

Conditioning of the calibration coefficients. To allow the more efficient direct (i.e. non-iterative) evaluation of large measurement data sets, the dependent and independent variables in the calibration coefficients defined in Eq. 11 and 12 are exchanged:

$$\phi = F(K_\phi, K_\gamma), \text{ and } \gamma = F(K_\phi, K_\gamma) . \quad (15)$$

The functions F are defined by the calibration data. The data of a 4-hole probe are shown in Fig. 17 to illustrate also the pitch sensitivity.

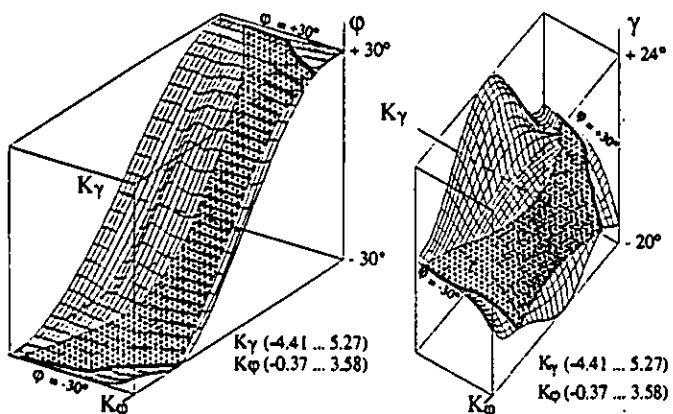


Fig. 17: Calibration surfaces ϕ (K_ϕ, K_γ) and γ (K_ϕ, K_γ) of a cylindrical 4-hole probe (KUPFERSCHMIED and GOSSWEILER 1992).

Each dot of the "stretched" mesh represents a calibration point. The fine-lined mesh is provided for visualization purposes only and does not affect the further data evaluation.

Modeling and accuracy. The calibration surfaces represented by Eq. 13, 14 and 15 are approximated by bivariable polynomials. For accuracy reasons, a third variable containing the Mach number dependency is not implemented; the Mach number is determined using an interpolation between the discretely calibrated Mach number steps. The degree of the polynomial depends on both the required angular range and on the desired accuracy. Practical limits for the degree are set by the CPU time for the later evaluation and by the number of data points available (a high degree of freedom is required for the least-squares approximation to avoid numerical oscillations).

Due to the large angular range required by fast-response measurement, the coefficient surfaces are rather complicated (e.g. Fig. 17, right), making a detailed error analysis necessary. The residuals of the angle evaluation model (Eq. 15) are shown in Fig. 18 for the cylindrical 4-hole probe when the calibration data are modeled to different degrees m, n and within different angular ranges.

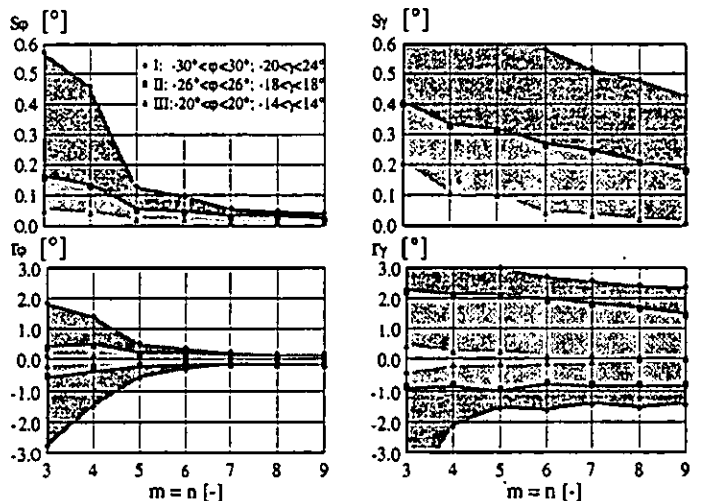


Fig. 18: Accuracy of the yaw and pitch angle evaluation model depending on polynomial degrees (m, n) and angular range.

For the case considered, polynomial degrees $m = n = 6$ are a good compromise: The standard deviation of the yaw residuals remains within 0.1° for all 3 angular ranges. The residuals of the pitch angle are more sensitive to the angular range ($0.05^\circ < r_\gamma < 0.6^\circ$). The extreme residuals (Fig. 18, bottom) are not only influenced by stochastic calibration errors, but also by systematic differences in some regions of the surfaces.

OPERATING CONCEPTS AND SYSTEM CONFIGURATION

Introduction. In order to achieve a high measurement accuracy with fast-response probes (e.g. velocity uncertainty below 1%), the system operating concepts require great attention: They specify the steps necessary in a given turbomachinery application to optimize the measurement system in terms of accuracy, reliability and gain of information. In the following, some basic operating concepts related to the FRAP® System are presented. To simplify the discussion, only 2D measurements are considered.

Probe operation modes

1-sensor probes operated in the *pseudo* 3-sensor mode. In this case, the fluctuating flow is measured time-resolved, at every probe traverse position under 3 angular positions of the probe shaft (Fig. 19). The time-averaged flow direction is preferably chosen as the center position φ_{FR} , but misalignments within a few degrees are acceptable. At this yaw position, sensor voltage data series $U_1(t)$, $U_{e1}(t)$ are collected over a large number m of rotor revolutions (typ. $m = 100 \dots 300$). Then the probe shaft is rotated to the $-\Delta\varphi_{FR}$ position and data acquisition is started at some arbitrary time Δt_1 , giving $U_2(t + \Delta t_1)$ and $U_{e2}(t + \Delta t_1)$. The same is done with the probe turned to the $+\Delta\varphi_{FR}$ position, giving U_3 , and U_{e3} , from Δt_{II} on. A value of $\Delta\varphi_{FR} = 43^\circ$ is well adapted to this cylindrical probe geometry, since the pressure tap measures about the (time-averaged) static pressure at this yaw angle position.

Using the sensor calibration data, the voltages are numerically converted into pressure (p_1 , p_2 , p_3) and temperature (T_1 , T_2 , T_3) time series, the latter being virtually constant values due to the large time constant of temperature measurement. This conversion concludes the "measurement" part, see Fig. 19.

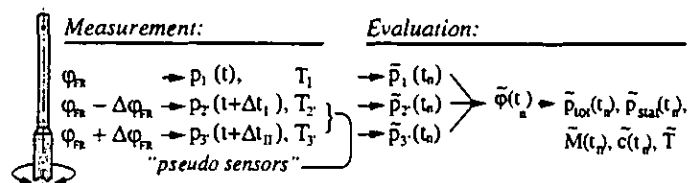


Fig. 19: 1-sensor probe used in the *pseudo* 3-sensor mode.

Each of the time series p_1 , p_2 , p_3 , typically comprises a steady ("DC") component and fluctuations ("AC") due to deterministic (rotor-position determined) and stochastic (e.g. turbulence induced) fluid dynamic events. By *ensemble averaging* (SHREEVE et al. 1978) based on a once-per-revolution trigger signal of the turbomachine shaft, all stochastic fluctuations are statistically eliminated and there remain three time series \bar{p}_1 , \bar{p}_2 , \bar{p}_3 , typical of any one rotor revolution $0 < t_N < 1/N$. In terms of shaft synchronized time t_N these series are simultaneous and may be combined like the signals of a 3-sensor probe (with sensors located at -43° , 0° , $+43^\circ$) to give all flow quantities, see Fig. 19.

Thus, the 1-sensor probe functions as a *pseudo* 3-sensor probe. The ensemble-average, marked with " \sim ", is defined as

$$\bar{p}(t_n) = \frac{1}{m} \cdot \sum_{i=1}^m p_i(t_n) \quad (16)$$

with $p_i(t_n)$ as the value of the pressure sensor i at the rotor-synchronized time t_n . Pressure fluctuations non-synchronous with the rotor (or its higher harmonics generated, e.g., by blade passing) contribute to the ensemble standard deviation:

$$\tilde{\sigma}(t_n) = \sqrt{\frac{1}{m} \cdot \sum_{i=1}^m (p_i(t_n) - \bar{p}(t_n))^2} \quad (17)$$

The data evaluation of these pressure signals provides the time-resolved ensemble-averaged flow quantities $\bar{\varphi}$, \bar{p}_{tot} , \bar{p}_{star} , \bar{M} , \bar{c} and \bar{T} at a given traverse position for one typical rotor revolution.

Determination of the pitch angle $\tilde{\gamma}$ requires at least one additional sensor or a 4-sensor probe. This is not treated here in detail.

The total number m of revolutions to be sampled determines the statistical uncertainty $\tilde{\sigma}_{uea}$ of the ensemble-averaged results:

$$\tilde{\sigma}_{uea} = \frac{\tilde{\sigma}(t_n)}{\sqrt{m}} = \sqrt{\frac{\sum (x_i(t_n) - \bar{x}(t_n))^2}{m \cdot (m-1)}} \quad (18)$$

Thus the accuracy can only be improved with the square root of the number of revolutions.

3-sensor probe mode. In this case a time-resolved measurement of the fluctuating flow is carried out at every traverse position under a single angular position φ_{FR} of the probe shaft (Fig. 20), and the signals of these sensors are collected simultaneously. Generally the center sensor tap will face the time-averaged flow direction. A correction of φ_{FR} by repeating the measurement may be necessary if the yaw angle distribution is strongly asymmetric.

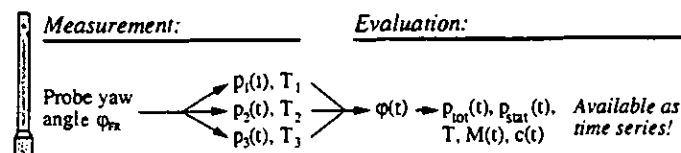


Fig. 20: Description of the 3-sensor probe mode.

The flow information is available as time series containing also the stochastic parts of the signal, such as turbulence. The drawback are the larger data acquisition equipment necessary for the additional sensors and the higher complexity of the data evaluation (e.g. larger angular fluctuations due to the stochastic contents have to be treated).

The experience with the FRAP® System applied to several industrial test turbomachines have shown that 1-sensor probe systems operated in the *pseudo* 3-sensor mode cover many demands. They are easier to handle during the calibration, the measurements and the data processing. However, more specific investigations like stall inception or operations in blow-down test facilities – where cross-correlated time-series are necessary – require the use of multi-sensor probes to collect the data of each pressure tap simultaneously. Flow direction probes accommodating up to 6 sensors have been developed for such applications and allow any flow yaw angle around the probe to be determined (RIESS and WALBAUM 1996).

Sensor adjustments

Although the probe's sensors are thoroughly calibrated in terms of temperature and pressure to meet the application's conditions, they are prone to drift and hysteresis effects. To fulfill the accuracy requirements, periodic checks of the sensor pressure-zero $K_z(t)$ and gain $K_g(t)$ drift are necessary in short time intervals, to allow a readjustment of the calibration characteristics in Eq. 7 by applying the correction:

$$\Delta p(U, U_e, t) = K_z(t) + K_g(t) \sum_{i=0}^m \sum_{j=0}^n k_{pij} U^i U_e^j \quad (19)$$

These operations are performed briefly prior and after traversing the flow path by retracting the probe into a recessed tower, where the conditions are monitored. Fig. 21 (left) shows a typical evolution of the residuals (standard deviation s_r and extreme values) of the pressure evaluation using Eq. 7 directly after calibration and in the following 4 temperature cycles in the computer-controlled sensor test facility.

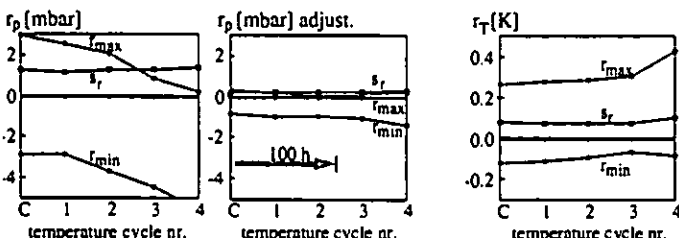


Fig. 21: Residuals of a sensor evaluation: during calibration (C) and the 4 following temperature cycles (FRAP® C1S18#12).

The residuals in Fig. 21 (center) illustrate the significant accuracy improvements when the pressure data are readjusted for each temperature cycle using Eq. 19. The temperature readings (Fig. 21, right) are not readjusted, since they were found to be stable over long time intervals.

Measurement system configuration

Overview. A fully computer-controlled probe control system has been developed (Fig. 22). The automation of all measurement sequences ensures an optimum probe operation for accuracy and timing, and further reduces errors by performing strictly repetitive operations.

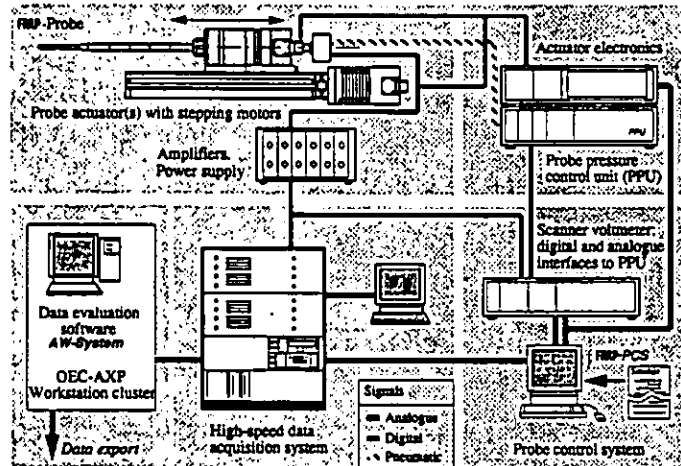


Fig. 22: Configuration of the FRAP® System for time-resolved measurements in turbomachines.

Hardware components of the FRAP® System. The system consists of the following components (KUPFERSCHMIED 1998):

- **Probe control system (PCS)** with a LabView™ software application controlling the specific measurement equipment
- **Probe pressure unit (PPU)** providing stable pressure levels to operate the sensors in the most effective pressure range independently of the pressure level in the turbomachinery flow.
- **Instrument amplifiers** in SMD technology mounted into the probe shaft end block to reduce the distance to the sensors.
- **High-speed data acquisition system** with a high gain and phase accuracy over the whole bandwidth. The rotor position reference is set by an optical trigger module.
- **High-precision 2-axis probe actuators** with stepping motor controllers used to traverse the probe through the flow passage.
- **Workstation(s) for off-line data evaluation**, connected by Ethernet to the high-speed data acquisition system.

System operation. All sequences for operating automatically the probes and other equipment in the target turbomachine are programmed in a "task file". Thus the measurement schedule can be optimized for the task and tested prior to measurement. This way high costs due to missed measurements or even hardware damage can be conveniently avoided.

MEASUREMENT DATA EVALUATION

The numerical evaluation of large time-series of sensor signals – with data acquisition throughputs of typ. 3.2 MB/s – to detailed distributions of flow quantities plotted over a traverse requires efficient handling and data processing capabilities. A general overview of the data evaluation is given in Fig. 23. The present software is an evolution of the "AW-System" package developed in-house specifically for large time series (HERTER et al. 1992). An open user interface provides a good interactivity, in order to monitor and control each evaluation step.

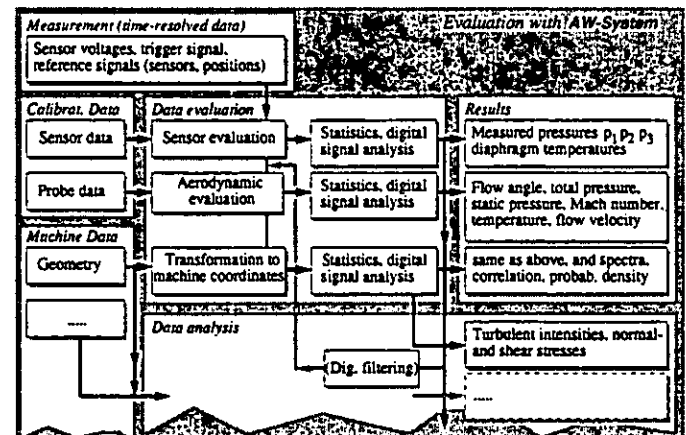


Fig. 23: Flow chart of the standard data evaluation software.

The **data analysis** – which aims at the detailed fluid dynamic analysis of the results and the feedback to turbomachinery development – is a further step in the data processing.

APPLICATIONS IN TURBOMACHINERY

The FRAP® System can be used for axial and centrifugal flow turbomachinery applications. Depending on the focus of the investigations, 1-sensor probes operated as pseudo 3-sensor probes or more complex 3 or 4-sensor probes can be used (e. g. if cross-correlated time-series are required such as for turbulence measurements, for stall inception or in blow-down test facilities). The present operating limits are given by the maximum temperature of 140° C, the analogue bandwidth of 45 kHz, the Mach number (0.15...0.8 under atmospheric conditions, extension planned) and the flow medium (gas). Thanks to the supplied reference pressure the system can cope with pressure levels up to several bar.

The FRAP® System has been integrated in several *in-house applications* such as a turbulent pipe flow (GOSSWEILER, HERTER, and KUPFERSCHMIED 1992) or an axial low-speed blower. It is routinely used in the centrifugal compressor test stand "Rigi" (reported in RODUNER et al. 1998 and in Part 2 and 3 of this paper). The *applications in industrial test facilities* includes measurements in the axial-flow test compressor of a turbojet engine and in an axial-flow research turbine (air). Close contacts with external institutions point toward an increasing interest in the quality data delivered by this technique.

CONCLUSIONS AND OUTLOOK

The development of fast-response aerodynamic probe measurement equipment at the Turbomachinery Laboratory of the ETH Zurich has resulted in a high-performance system primarily dedicated to turbomachinery applications. All components of this FRAP® System – including miniature probes, signal amplifiers, data acquisition electronics, calibration facilities and data processing – have been individually optimized with respect to the measurement accuracy (AC and DC), to the system flexibility and the operating efficiency. Especially the 1-sensor probes operated as pseudo 3-sensor probes have shown a high potential, because they combine the simple application and evaluation methods with a good return of information about the time-resolved flow patterns.

The current improvement of selected components make the FRAP® System suited for more complex applications, such as detailed 2D flow field measurements or even 3D with 4-sensor probes. The system has been successfully used for measurement campaigns in different turbomachines at the ETH and in industrial test facilities. Several new applications are planned in house and at other institutions.

REFERENCES

- Ainsworth, R.W., Allen, J.L., Batt, J.J.M., 1995, "The development of fast-response aerodynamic probes for flow measurements in turbomachinery", *ASME Journal of Turbomachinery*, Vol. 117/4
- Arts, T., Dénos, R., Brouckaert, J.-F., and Popp, O., 1996, "The dual hot wire aspirating probe", *Proc. 13th Symp. on Meas. Tech. for Transonic and Sup. Flows in Cascades and Turbomachines*, Zürich
- Chue, S.H., 1975, "Pressure probes for fluid measurement", *Prog. Aerospace Sci.*, Vol 16, No. 2, 147-223
- Cook, S.C.P., 1989, "Development of a High Response Aerodynamic Wedge Probe and Use in a High Speed Research Compressor", *Proc. 9th Int. Symp. on Air Breathing Engines*, ISABE 89-7118, Athen
- Epstein, A.H., 1985, "High Frequency Response Measurements in Turbomachinery". *Measurement Techniques in Turbomachines, VKI Lecture Series 1985-03*, VKI, Rhode-Saint-Genèse, Belgium
- Gizzi, W.P., and Gyarmathy, G., 1998, "Correction of time-dependent aerodynamic measurement errors of fast-response probes", *Proc. 14th Symp. on Meas. Tech. for Transonic and Supersonic Flows in Cascades and Turbomachines*, Limerick, Ireland
- Gossweiler, C., Herter, D., and Kupferschmied, P., 1992, Fast-Response Probe Measurements in a Turbulent Pipe Flow, *Proc. 11th Symposium on Measuring Techniques for Transonic and Supersonic Flows in Cascades and Turbomachines*, Munich
- Gossweiler, C., Humm, H.J., and Kupferschmied, P., 1990a, "The Use of Piezo-Resistive Semi-Conductor Pressure Transducers for Fast-Response Probe Measurements in Turbomachinery", *Proc. 10th Symp. on Meas. Tech. for Transonic and Supersonic Flows in Cascades and Turbomachines*, VKI Brussels
- Gossweiler, C., Humm, H.J., and Kupferschmied, P., 1990b, "Dynamic Calibration of Piezoresistive Pressure Transducers in the Frequency Range of over 500 kHz", *Proc. Micromechanics Europe 1990*, Berlin
- Gossweiler, C., Kupferschmied, P., and Gyarmathy, G., 1995, "On Fast-Response Probes, Part 1: Technology, Calibration and Application to Turbomachinery", *ASME Journal of Turbomachinery*, Vol. 117/4
- Humm, H.J., 1996, "Optimierung der Sondengestalt für aerodynamische Messungen in hochgradig fluktuierenden Strömungen", PhD Thesis ETH Nr. 11661, Zurich (in german)
- Humm, H.J., Gossweiler, C., and Gyarmathy, G., 1995, "On Fast-Response Probes, Part 2: Aerodynamic Design Studies", *ASME Journal of Turbomachinery*, Vol. 117/4
- Heneka, A., 1983, "Entwicklung und Erprobung einer Keilsonde für instationäre dreidim. Strömungsmessungen in Turbomaschinen". *Mitteilungen des Institutes Nr. 14*, IT'S, University of Stuttgart, Germany
- Herter, D., Chrisander, N.O., and Gossweiler, C., 1992, "AW-System – An Interactive Environment for the Evaluation of Large Time Series", *Proc. 11th Symp. on Meas. Tech. for Transonic and Supersonic Flows in Cascades and Turbomachines*, Munich
- Hinze, J. O., 1975, "Turbulence", Second Edition, McGraw-Hill, New York
- Kerrebrock, J.L., Epstein, A.H., Haines, D., and Thompkins, W.T., 1974, "The MIT Blowdown Compressor Facility", *Transactions of the ASME*, October 1974
- Kerrebrock, J.L., Thompkins, W.T., and Epstein, A.H., 1980, "A Miniature High Frequency Sphere Probe", in "Measurement Methods in Rotating Components of Turbomachinery", Lakshminarayana and Rundtadler, eds., ASME New York
- Kovasznay, L.S.G., Tani, I., Kawamura, M., and Fujita, H., 1981, "Instantaneous Pressure Distribution Around a Sphere in Unsteady Flow", *J. of Fluids Eng.*, 103, December 1981
- Krause, L. N., and Dudzinski, T.J., 1969, "Flow-Direction Measurement with fixed Position Probes in Subsonic Flows over a Range of Reynolds Numbers", *NASA TMX-52576*, May
- Kupferschmied, P., 1998, "On the Methodology of Time-Resolved Measurements with Aerodynamic Probes in Compressors and Turbines", PhD Thesis ETH Nr. 12774, Zurich (in german)
- Kupferschmied, P., and Gossweiler, C., 1992, "Calibration, Modelling and Data Evaluation Procedures for Aerodynamic Multihole Pressure Probes on the Example of a Four Hole Probe", *Proc. 11th Symp. on Meas. Tech. for Transonic and Supersonic Flows in Cascades and Turbomachines*, Munich
- Kupferschmied, P., Roduner C., and Gyarmathy G., 1998, "Some Considerations on Using Miniature Fast-Response Aerodynamic Probes for Flow Temperature Measurements", *Proc. 14th Symp. on Meas. Tech. for Transonic and Supersonic Flows in Cascades and Turbomachines*, Limerick, Ireland
- Larguier, R., 1985, "Experimental Analysis Methods for Unsteady Flows in Turbomachines", ONERA, ISABE 85-7030
- Lisec, Th., Kreutzer, M., and Wagner, B., 1996, "Surface micromachined piezoresistive pressure sensors with step-type bent and flat membrane structures", *IEEE Trans. on electron. devices*, Vol. 43, No. 9
- Mailon, J.R., and Bernstein, H., 1983, "Temperature Compensation and Shunt Calibration of Semiconductor Pressure Transducers", *12th Transducer Workshop*, Melbourne (Fla.)
- Muntwyler, M., 1997, Personal communication, 26. 9. 97, Unisensor AG, Rickenbach-Attikon, Switzerland
- Ng, W.F., and Epstein, A.H., 1983, "High-frequency temperature and pressure probe for unsteady compressible flows", *Rev. Scientific Instrumentation* 54 (12)

Riess, W., Walbaum, M., 1996, "Initiation and propagation of flow instabilities in multi-stage axial compressor", *AGARD PEP 85th Symposium*, May 1995, CP-571

Roduner, C., Köppel, P., Kupferschmied, P., and Gyarmathy, G., 1998, "Comparison of measured integral averages at the impeller exit of a centrifugal compressor measured with both pneumatic and fast-response probes", *ASME Turbo Expo '98*, 98-GT-241, Stockholm

Shreeve, R. P., Simmons, J. M., West, J. C., and Winters K. A. 1978, "Determination of Transonic Compressor Flow Field by Synchronised Sampling of Stationary Fast Response Transducers", *Nonsteady Fluid Dynamics*, Ed. Crow D. E.; Miller J. A.; ASME 1978, 91-102

Smouth, P.D., 1996, "Probe installation and design criteria", *Temperature Measurements, VKI Lecture Series 1996-07*, von Karman Inst. f. Fluid Dynamics, Rhode-Saint-Genèse, Belgium

Strazisar, A.J., 1993, "Laser Anemometer Applications in Turbomachinery", *Proc. of the 2nd Intern. Symp. on Experimental and Computational Aerothermodynamics of Internal Flows*, Prag

Treaster, A.L., and Yocom, A.M., 1979, "The Calibration and Application of Five-Hole Probes", *ISA Transactions* Vol. 18, No. 3

Van Zante, D.E., Suder, K.L., Strazisar, and A.J., Okiishi, T.H., 1995, "An Improved Aspirating Probe for Total-Temperature and Total-Pressure Measurements in Compressor Flows", *ASME Journal of Turbomachinery*, Vol. 117, No. 4